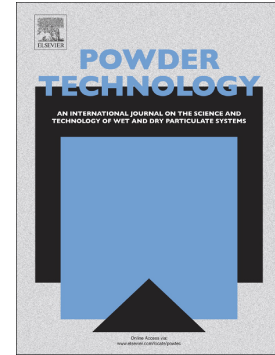


Journal Pre-proof

Evidence for the synthesis of La-hexaaluminate from aluminum-containing saline slag wastes: Correction of structural defects and phase purification at low temperature

J.J. Torrez-Herrera, E.G. Fuentes-Ordoñez, S.A. Korili, A. Gil



PII: S0032-5910(20)30844-5

DOI: <https://doi.org/10.1016/j.powtec.2020.08.087>

Reference: PTEC 15791

To appear in: *Powder Technology*

Received date: 4 March 2020

Revised date: 20 August 2020

Accepted date: 26 August 2020

Please cite this article as: J.J. Torrez-Herrera, E.G. Fuentes-Ordoñez, S.A. Korili, et al., Evidence for the synthesis of La-hexaaluminate from aluminum-containing saline slag wastes: Correction of structural defects and phase purification at low temperature, *Powder Technology* (2020), <https://doi.org/10.1016/j.powtec.2020.08.087>

This is a PDF file of an article that has undergone enhancements after acceptance, such as the addition of a cover page and metadata, and formatting for readability, but it is not yet the definitive version of record. This version will undergo additional copyediting, typesetting and review before it is published in its final form, but we are providing this version to give early visibility of the article. Please note that, during the production process, errors may be discovered which could affect the content, and all legal disclaimers that apply to the journal pertain.

© 2020. This manuscript version is made available under the CC-BY-NC-ND 4.0 license <http://creativecommons.org/licenses/by-nc-nd/4.0/>

Evidence for the synthesis of La-hexaaluminate from aluminum-containing saline slag wastes: correction of structural defects and phase purification at low temperature

J.J. Torrez-Herrera, E.G. Fuentes-Ordoñez, S.A. Korili, A. Gil

INAMAT²-Departamento de Ciencias, Edificio de los Acebos, Universidad Pública de Navarra, Campus de Arrosadía E-31006 Pamplona, Spain

Abstract

The synthesis of a lanthanum hexaaluminate from the aluminum extracted from a saline slag waste is presented for the first time. Briefly, a refluxing 2 M solution of HCl is used to extract the aluminum, giving $8.9 \text{ g}_{\text{Al}}/\text{cm}^3$ along with other metals in lower concentrations. This solution is used to synthesize the hexaaluminate by mixing with a stoichiometric amount of lanthanum nitrate. The results showed the formation of pure phase hexaaluminate at 1473 K, as well as predominance of the hexaaluminate phase at temperatures of 1273 and 1373 K. These results also indicate that the pure hexaaluminate phase can be obtained at a much lower temperature than when commercial aluminum solutions are used improving the applications as catalyst and thermal barrier material. It was also found that the presence of other metals in solution allows the structural problems and purity of the La-hexaaluminate phase to be corrected when working with stoichiometric ratios.

Keywords: aluminum industrial wastes, waste valorization, hexaaluminate, saline slags

1. Introduction

Aluminum is a non-ferrous metal used in a large number of applications and in a wide range of products. However, unlike other metals, aluminum can be almost completely recycled into new products by melting [1]. When these melting processes are carried out on an industrial scale, tilting rotary furnaces and salts are used. This results in the generation of saline slag wastes, which are classified as hazardous wastes [2,3]. The composition of these saline slags depends on the quality of the material being recycled and the amount of salt added to the furnace. In general, three fractions can be differentiated in saline slags, namely salts (NaCl + KCl), aluminum metal and a fraction of non-metallic oxides. Recovery of the waste involves separating each of these fractions and providing them with an application [4,5]. The non-metallic oxides fraction has been found to contain Fe_2O_3 , SiO_2 , Na_2O , AlN , Al_2O_3 , NaCl , MgO , Al_2O_3 , traces of KCl , cryolite (Na_3AlF_6), aluminum carbide (Al_4C_3) and small amounts of fluoride and chloride. Additionally, the presence of other components, such as MgF_2 , NaAlCl_4 , KAlCl_4 , MgO , KMgF_3 and K_2NaAlF_6 , has also been reported [2,5-7]. The aluminum present in the slags can be extracted by alkaline or acid leaching to synthesize other interesting materials such as zeolites and layered double hydroxides, developed by our research group [8,10]. In the case of acid leaching, which involves treatment with HCl at low concentrations, several species, such as Al^{3+} , Fe^{3+} , Ca^{2+} , Mg^{2+} , Na^+ and chlorides, amongst others, can be extracted in solution [2,6].

Hexaaluminates are a family of hexagonal aluminate compounds that have a unique layered structure comprising alternating spinel blocks with closed packed array of oxide ions and mirror planes. The general formula is $\text{AB}_x\text{Al}_{12-x}\text{O}_{19}$, where A can be a cation such as Na , Ba , La , Ca , Sr , Ce , amongst others. Component B represents a transition metal (Mn , Fe , Co , Cu , Ni , etc.) or noble metal ion (Ir , Ru , Pd , Rh), which can partially or completely replace the Al positions in the crystallographic structure [11,12]. The spinel blocks are composed only of Al^{3+} and O^{2-} ions and have the same rigid structure as the spinel. Large cations such as Na^+ , K^+ , Sr^{2+} and La^{3+} are found in the spacious mirror plane. The charge and radius of these cations mean that hexaaluminates have a $\beta\text{-Al}_2\text{O}_3$ or magnetoplumbite (MP)-type structure [13].

Several methods for the synthesis of hexaaluminates have been reported: solid state reaction [14,15], sol-gel [14,16,17], co-precipitation [18,19], reverse

microemulsion [20,21], nitrate decomposition [22-24], hydrothermal synthesis [25], carbon template [26,27], freeze drying [28,29], among others. The decomposition of nitrates is a simple method, since it consists of adding the aqueous solutions of the salts to a mixture of polyethylene glycol-isopropanol, after a reaction time, which may be under pressure, the drying and calcination steps are continued. Based on this method, the synthesis of hexaaluminates from an aluminum solution extracted from saline slag wastes is developed in this work.

Hexaaluminates have been used as catalytic supports for several reactions, such as combustion of VOCs, partial oxidation and dry reforming of methane, amongst others [30-33], with catalytic behaviors and properties being reported in terms of yield, selectivity and stability. Lanthanum hexaaluminate (LHA) has a high resistance to deactivation by coke deposition, and has therefore been suggested by several authors to be a very interesting catalyst for the above type of reactions [11,18,22,34]. Other applications of great interest for this type of material are as ceramic coatings and, recently, as a thermal barrier in turbines and jet engines in aircraft. Due to its thermal stability at high temperature and against hot corrosion, it is an alternative material to the zirconium typically used in these processes [35-37].

In this work, aluminum extracted from saline slag wastes using aqueous HCl solutions is used as an alternative aluminum source for the synthesis of hexaaluminates for the first time. The aluminum solutions were used as precursors in combination with lanthanum to obtain hexaaluminates with a molar La/Al ratio of 1:11. The presence of other metals in the extracted solution means that the hexaaluminate structure can be formed at a lower temperature than that reported when Al and La from commercial solutions are considered.

2. Experimental

2.1. Materials and aluminum extraction

Lanthanum(III) chloride heptahydrate (99.9%, Sigma Aldrich), 2-propanol (99.5%, Sigma Aldrich) and polyethylene glycol 400 (Merck) were used.

Aluminum was extracted from saline slags using the following procedure: 50 g of saline slag was added to 750 cm³ of an aqueous reagent solution (HCl 2M) in a reflux system consisting of a 1000 cm³ erlenmeyer flask with tube condenser, thus avoiding

volume losses. The slurries were heated to 373 K and kept at that temperature for 2 h. The solution was then allowed to cool and separated by centrifugation. The most important constituents of the filtered solution were determined by ICP-OES, using a VARIAN ICP-OES VISTA MPX with radial vision. The results obtained are summarized in Table 1. The composition of the aluminum saline slags before extraction (see Table 2) was determined by X-ray fluorescence (XRF), (through calibrated lines using well-characterized international minerals and semiquantitative for La through the measurement of a set of scans) in a PANalytical AXIOS instrument. For these results, low limits of detection for major elements were in the range of 0.01 wt.%, and approximately 10 ppm for trace elements.

2.2. Hexaaluminate synthesis

Based on the nitrate decomposition method and hydrothermal synthesis, our research group has developed the synthesis method described below, denoted as Alcohol Dilution (AD), in which 250 mL of the acid solution with aluminum extracted from the saline slags was concentrated serving as a matrix where the other reagents are added. The extracted aluminum solution was heated to reduce its volume fivefold (50 mL), thus giving a concentrated solution for hexaaluminate synthesis. A quantity of lanthanum chloride corresponding to a molar La/Al ratio of 1:11 was dissolved in 200 mL a mixture of isopropanol, polyethylene glycol in a 1/1 volumetric ratio. The mixture of alcohols was added to the aluminum solution slowly, with vigorous stirring, over 30 minutes, then poured into a 250 mL stainless steel autoclave reactor and heated at 473 K for 16 h. The resulting product was dried in an oven until the liquid matrix had been eliminated, then calcinated at a heating rate of 10 K/min to 673 K for 1 h, and then successively to several temperatures between 873 and 1473 K for 2 h to study the structure evolution.

2.2.1. Characterization techniques

The structural phases were analyzed using an X-ray diffractometer (model Siemens D5000) equipped with an Ni-filtered CuK α radiation source ($\lambda = 0.1548$ nm). The main textural properties of the solids were determined by nitrogen adsorption at 77 K using a Micromeritics ASAP 2020 Plus adsorption analyzer. The chemical

composition of the sample was determined semiquantitatively by X-ray fluorescence (XRF) using a PANalytical AXIOS instrument. The programmed reduction temperature was measured using a Micromeritics TPR/TPD 2900 device and the infrared spectra of the samples calcined at several temperatures using a Jasco FT/IR-4700 spectrometer. Finally, the morphological analysis and chemical composition of the sample were carried out using a SEM Phenom Pro Desktop and an HR-TEM JEOL JEM 2100F.

3. Results and discussion

The material synthesized using La and aluminum extracted from saline slags, and calcined at 1473 K, was characterized by XRD and the pattern obtained is shown in Figure 1. According to the extraction of multimetal oxides, and the presence of La and Ca, the most probable hexaaluminate structure, and that which best fits the existing patterns, appears to be magnetoplumbite. Indeed, hibonite-Ca (pattern # 00-007-0785), which is a type of magnetoplumbite, is the structure in closest agreement with the synthesized sample.

The hexaaluminate synthesized was calcined at various temperatures to evaluate how the structure evolves with temperature. The X-ray diffractograms of the samples at several temperatures are also presented in Figure 1. Thus, the sample calcined at 873 K (a) presents an amorphous phase that appears to be similar to minerals from the spinel group of alumine (pattern # 00-021-1152), most likely due to the presence of a mixture of MgO, MnO and FeO, with Al₂O₃. Upon calcination of the sample at 1073 K (b), the spinel and the additional metal oxides begin to transform into the hexaaluminate phase hibonite-Ca (pattern # 00-007-0785), as shown by the appearance of diffraction lines related to this oxide. Calcination at 1273 K (c) results in a decrease in the intensity of the diffraction lines for the spinels seen at lower temperatures and an increase in the intensity of the hexaaluminate peaks. The diffractograms for samples (b) and (c) are complex due to the mixture of components and crystallographic phases. For sample (d), which was calcined at 1473 K, the spinel phase has disappeared almost completely and high correspondence with the hexaaluminate is found. As such, the hexaaluminate has almost completed its

transformation at this temperature since the diffraction lines obtained are well defined.

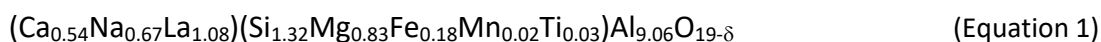
LHA exhibit a double Frenkel defect, which hinders formation of the hexaaluminate phase with a molar La:Al ratio of 1:11. This defect can be corrected if the amount of aluminum is increased to around 14-15 with respect to lanthanum. As such, a predominant hexaaluminate phase can be obtained, with an aluminate phase as a secondary, although not pure, phase even when increasing the calcination temperature to 1723 K [38,39]. Rao and Mariappan [38] studied the structural formation of LHA, comparing two synthesis methods and using molar La:Al proportions of 1:11, 1:12 and 1:15. Samples were calcined at 1723 K for 2 h, obtaining a high crystallinity with very well defined peaks in all three cases. The aluminate phase was found to be predominant for the molar ratios 1:11 and 1:12, with the hexaaluminate phase being secondary. In the case of the sample obtained with a 1:15 molar ratio, a predominant hexaaluminate phase was observed, with the aluminate phase being secondary in this case. No pure phases were obtained at this temperature. Park et al. [39] showed that LHA is more likely to be a non-stoichiometric phase corresponding to $\text{La}_{0.83}\text{Al}_{11.83}\text{O}_{19}$ or $\text{LaAl}_{11.67}\text{O}_{19}$ with a molar Al/La ratio in the range 13-14. These authors also predicted that these two phases, which have an MP structure, may form solid solutions. Modeling also revealed the possible existence of metastable phases. They explained the structural defect observed using two types of defect models: a “vacancy model” and an “interstitial oxygen model” [39].

In the case of the hexaaluminate obtained from the saline slags using a molar La:Al ratio of 1:11, a pure phase with high densification of the solid was obtained at 1473 K. This finding shows that the saline slags solution self-corrects the double Frenkel structural defect. A stoichiometric ratio, and the metallic synergy of the components, makes it possible to obtain the hexaaluminate phase at lower calcination temperatures. This may be due to the fact that a lower diffusion energy is needed in the solid-state reaction in the presence of other metals. Acid treatment of the saline slags allows other metals, such as Mg, Fe, Si, Mn and Ti, which work in excellent synergy with La to obtain the hexaaluminate, to be extracted.

In order to corroborate that the hibonite autocorrects the structural defect Frenkel in LHA, two samples with commercial precursors were synthesized and calcined at 1473 K for 2 h. The samples were AD1, mole La/Al ratio of 1:11, and AD2, mole La/Al/Ni ratio of 1:15:0.25. The XRD patterns are included in Figure 2. It can be seen that the hexaaluminate structure is not achieved when using a mole La/Al ratio of 1:11 (AD1). Under these conditions, the predominant phase is La(AlO₃) due to the vacancies generated by the double Frenkel effect in LHA, possibly due to the repulsive effects of La³⁺ on Al³⁺ that prevents it from migrating within the structure and to form a hexagonal arrangement corresponding to the LHA phase. On the contrary, it can also be seen that the hexaaluminate phase develops for sample AD2. This result can be explained by the presence of an excess of Al³⁺ and Ni²⁺. The addition of nickel allows the formation of the MP-type hexaaluminate structure and reduce the secondary phases of aluminate to 1473 K, an effect reported by Rao and Mariappan [38]. This result demonstrates the synergistic effect of metals and the correction of the defect by using Al extracted from saline slags, since other metals that carry this effect are also extracted.

The quantitative chemical composition by of the sample synthesized, as determined by FXR (low limits of detection for major elements are in the range of 0.01 wt.%, and approximately 10 ppm for trace elements) and SEM-EDX (determined by EDX-mapping from an average of 20 measurements on the sample with a percentage measurement uncertainty of 0.5 wt.%), is shown in Table 3 and Figure 3. These values allow an atomic relationship between the main elements that may be present to be established. The table shows a possible composition in groups according to the general hexaaluminate formula AB_xAl_{12-x}O₁₉, where A represents cations such as La, Ca, Na and B represents metals that replace Al in the structure, such as Mg, Fe, Si, Ti and Mn. The hibonite formula shown in Equation 1 can therefore tentatively be proposed, assuming that this oxide is only obtained in the final sample. Although the sum of cations (A) in the hibonite formula must be 1, and a value of more than 2.29 is obtained, this may be possible in the case of hexagonal structures with values of metallic cations greater than 1 due to the presence of cations such as Ca and Na. The formation of Ca₂Al₁₂O₁₉ has recently been proposed via a solid-state reaction [40-42]. In addition, Fe can

replace Al completely in a hexaaluminate and convert it to hexaferrite [12,43], therefore both structures could be comparable. In the case of hexaferrites, several examples of structures containing large cations with molar ratios greater than 1, such as $\text{Ba}_2\text{Fe}_{12}\text{O}_{19}$ [44,45], $\text{Ba}_2\text{Cu}_2\text{Fe}_{12}\text{O}_{22}$, $\text{Ba}_2\text{Fe}_2\text{Fe}_{12}\text{O}_{22}$ (type Hexaferrite Y) [44-47], which still remain in the hexagonal phase, are known.



The specific surface and pore volume values at several temperatures, and the predominant phase at those temperatures, can be found in Table 4. The S_{BET} results at 1473 K suggest that almost complete sintering is achieved as a result of the applied synthesis mechanism, thus resulting in a high densification. It is important to mention that the predominant hexaluminate phase is observed at 1373 K, with excellent purity and acceptable porosity for use as catalytic support, thus representing a reduction in the formation temperature. The size of the crystallite was determined using the Debye–Scherrer equation. Evolution of the crystallite size was observed, with uniform growth of the crystallite, thus confirming an excellent densification. In addition, a sintering process that occurs at very low temperatures can be proposed, since the process starts with a low S_{BET} value compared to alumina and a small crystallite size. As such, the synergy of the same slag components may benefit diffusion of the species, thus resulting in high densification, high diffusion in the solid state and low porosity, which allows the phase transformation to occur at a lower temperature.

The decrease in porosity with calcination temperature is shown in Figure 4, and the corresponding changes in transformations of the spinel phases become clear when applying the derivative of the curve. It can also be seen that the enrichment range of the LHA phase occurs between 1273 and 1373 K, where the derivative remains almost constant, whereas the slope changes completely at the temperature at which the pure phase appears (1473 K).

When La reacts with other metals it exhibits different structural mechanisms in the synthesis of hexaaluminates, with these mechanisms being conditioned by the

nature of the metals, as well as by the stoichiometric ratio in which they are present. This has a significant effect on the structure of the final material, the temperature required to form it, the type of phase that is formed, as well as on the textural properties. This behavior was proposed and discussed by Zhang et al. [12], who studied the evolution of the crystal structure with temperature and the crystallographic centers of $\text{LaFe}_x\text{Al}_{12-x}\text{O}_{19}$ -type hexaaluminates synthesized using a co-precipitation method with commercial precursors. These authors modified the Fe concentration ($x = 0-12$) and calcined the materials at several temperatures (between 973 and 1673 K), finding various phase compositions with variations in the Fe concentration, which competes with Al at the structural centers. Thus, for a value of $x = 0$, they found MP/ LaAlO_3 as phases, whereas for a value of x between 1 and 7 they observed the MP phase, for a value of x between 8 and 11 MP/ $\alpha\text{-Fe}_2\text{O}_3$ phases and, finally, for a value of $x = 12$ they found $\alpha\text{-Fe}_2\text{O}_3/\text{LaFeO}_3$ phases. They also proposed that Fe is able to substitute Al in the spinel block. The same authors [48] synthesized the hexaaluminate $\text{BaFe}_x\text{Al}_{12-x}\text{O}_{19}$ by varying the Fe concentration ($x = 0-12$) and found that the structural phase was transformed from $\beta\text{-Al}_2\text{O}_3$ to MP as the Fe concentration increased.

Machida et al. [49] and Groppi et al. [50] investigated $\text{BaMn}_x\text{Al}_{12-x}\text{O}_{19}$ catalysts and found that replacement of aluminum with manganese up to $x \approx 3$ was possible and that additional phases, such as perovskite, spinel, etc., are produced if this ratio is increased. Wang et al. [51] and Tian et al. [13] studied substituted materials and obtained $\text{LaMn}_x\text{Al}_{12-x}\text{O}_{19}$ with a maximum value of $x = 1$. They also found that LaMnO_3 formation occurred after the addition of additional Mn. This behavior may be associated with the limited ability of hexaaluminate to incorporate other metal ions into the structure.

The relationship between the decrease in porosity and crystallite size are shown in Figure 5 (a), which allows the effect of the phase transformation on the specific surface to be identified since the spinel phase undergoes changes towards the hexaaluminate phase. In the solid matrix, the competition between species such as Fe-Al to occupy the same structural centers generates this inverse correspondence between the crystallography and the textural properties for the hexaaluminate synthesized. This same phenomenon was observed by Zhu et al. [48], who reported that the variation in Fe concentration in $\text{BaFe}_x\text{Al}_{12-x}\text{O}_{19}$ generates a destructive effect

on porosity related to competition for the aforementioned octahedral centers, finding specific surface values of between 20 and 4 m²/g for values of x between 0 and 9. For values of x greater than 9, the specific surface is zero.

The relationship between specific surface area and crystallite size and temperature are also shown in Figure 5 (b), which was created using the Krigin–Gridding interpolation method and according to the following model (Equation 2):

$$S_{BET} = \frac{846.189 - 0.667T + 24.577SG - 6.4677SG^2 + 0.3604SG^3}{1 - 0.01516T + 5.6945T^2 - 3.6677T^3 + 1.2670SG - 0.03177SG^2} \quad (\text{Equation 2})$$

where T is the calcination temperature and SG the crystallite size. This model gives an R² value of 0.992 and a χ^2 value of 1.05, thus showing that the model fits the data very well.

The reduction profiles of the hexaaluminates calcined at various temperatures are shown in Figure 6. It can be seen that materials calcined at 873 and 1073 K present reduction processes over a wide temperature range (between 570 and 1173 K), with this behavior being related to the reduction of species that have not yet been incorporated into the hexaaluminate structure. Once the hexaaluminate phase has formed and predominates, in other words for samples calcined above 1273 K, there is no evidence of reduction processes. These findings indicate that there are no reducible species outside the structure and that the Fe and Mn extracted from the starting saline slags (see Table 2) have been fully incorporated into the hexaaluminate structure. It should also be noted that the reducible oxides that contribute to H₂ consumption are those related to Fe species, and to a lesser extent to Mn species, given that La, Al, Ca and Mg oxides are not reducible. The reduction profile of the sample calcined at 873 K shows four reduction maxima at 593, 713, 773 and 913 K. The first can be attributed to the reduction Mn₂O₃ to Mn₃O₄, the second to the reduction of Mn₃O₄ to MnO and Fe₂O₃ to Fe₃O₄, and the third to the Fe species that migrate from Fe₃O₄ to FeO. Finally, the latter corresponds to the transition from FeO to metallic Fe since MnO is not reducible under these conditions [52,53]. The sample calcined at 1073 K shows the typical behavior described by Leith and Howden [53] for materials based on Fe and Mn oxides. In this case, the species are reduced at higher temperatures due to interactions with the metallic support. In view of the temperature profile, reduction maxima can be

assigned to the temperatures 713, 780, 876 and 995 K. The correspondence of species would be with those described above.

The evolution of the structure of the hexaaluminate as a function of calcination temperature was also characterized by FTIR and is shown in Figure 7, which shows a broad band centered at 3440 cm^{-1} and another at 1640 cm^{-1} assigned to the characteristic stretching and bending vibrations of OH groups, respectively. These bands are associated with water adsorbed on the samples, and experience a decrease in intensity with increasing calcination temperature, which may be related to the loss of surface area inherent to the process [54]. All spectra shows bands in the range $400\text{--}1000\text{ cm}^{-1}$ assigned to the vibration of metal-oxygen bonds (M-O). In the presence of multiple metals, the increase in calcination temperature means that hexaaluminate structure formation results in narrower and better defined bands [54,55]. In all cases, bands due to tetrahedral $[\text{AlO}_4]^{5-}$ stretching vibrations, specifically the shoulders in the spectra at 750 cm^{-1} , are evidence of this kind of site. Octahedral $[\text{AlO}_6]^{9-}$ stretching vibrations appear at 695 cm^{-1} and as a shoulder at 578 cm^{-1} [54,55]. Bands due to M-O bonds other than to Al can be observed in the spectra, including the Mg-O bond vibration at 840 cm^{-1} [55], Fe-O at 455 cm^{-1} [55-57], and, finally, the sample calcined at 1473 K exhibits characteristic peaks for hibonite La-Ca at 520 , 660 and 980 cm^{-1} [55,58].

The SEM-TEM image of the hexaaluminate calcined at 1473 K is shown in Figures 3 and 8. From Figure 3, there are an agglomeration of the hexaaluminates which causes a high densification and a low porosity [59]. It is not observed that the microcrystals are sintered since they keep their microstructure very well defined and independent of each other. In the diffractogram included in Figure 1, a high crystallinity of the sample was observed, which could be related to the excellent structural definition that can be seen. In addition, an aluminate secondary phase was practically not observed, which would allow establishing a high phase purity, conditioning with the SEM images and with the composition determined by EDX mapping (20 measurements on the sample and an average composition with a percentage uncertainty of the measurement of 0.5%). TEM-SAED images of the hexaaluminates obtained are also included in Figure 8. In this figure is possible to see

the atomic distribution of the hexagonal arrangements in the microstructure and the interplanar lattice patterns corresponding to LHA.

4. Conclusion

The synthesis of hexaaluminate and La-Ca hibonite from aluminum extracted from an aluminum saline slag has been presented for the first time. The proposed procedure is suitable for upgrading a hazardous industrial waste and obtaining a material that can have various uses as a catalyst and thermal insulator.

The aluminum used in the synthesis of hexaaluminate is extracted from saline slags in an acid medium, a process that allows the extraction of smaller quantities of other metals. The presence of these metals provides great advantages in the synthesis of hexaaluminates since it allows to obtain the hexaaluminate phase with a stoichiometric La/Al ratio at lower temperatures than another hexaaluminates reported, and with a greater degree of phase purity than if the synthesis is carried out using commercial reagents.

Credit authorship contribution statement

In this work, Mr J.J. Torrez-Herrera carried out the experiments, analyzed results and involved in writing/revising manuscript; Dr E.G. Fuentes-Ordoñez and Prof S.A. Korili analyzed results and involved in writing/revising manuscript; Prof. A. Gil provided conceptualization, project administration, manuscript writing and revision guidance.

Declaration of competing interest

The authors declare that they have no known competing financial interests or personal relationships that could have appeared to influence the work reported in this paper.

Acknowledgements

The authors are grateful for financial support from the Spanish Ministry of Economy, Industry and Competitiveness (AEI/MINECO), the European Regional Development Fund (ERDF) through project MAT2016-78863-C2-R. JJTH thanks

Universidad Pública de Navarra for a pre-doctoral grant. AG and EGFO also thank Santander Bank for funding via the Research Intensification Program.

Journal Pre-proof

5. References

- 1 T. Tolaymat, X. Huang, Secondary aluminum processing waste: salt cake characterization and reactivity, U.S. Environmental Protection Agency, Washington, DC, EPA/600/R-15/109, 2015.
- 2 B. Dash, B.R. Das, B.C. Tripathy, I.N. Bhattacharya, S.C. Das, Acid dissolution of alumina from waste aluminium dross, *Hydrometallurgy* 92 (2008) 48-53.
- 3 M. Mahinroosta, A. Allahverdi, Enhanced alumina recovery from secondary aluminum dross for high purity nanostructured γ -alumina powder production: Kinetic study, *J. Environ. Manag.* 212 (2018) 278-291.
- 4 N. Ünlü, M.G. Drouet, Comparison of salt-free aluminum dross treatment processes, *Resour. Conserv. Recycl.* 36 (2002) 61-72.
- 5 A. López-Delgado, H. Tayibi, Can hazardous waste become a raw material? The case study of an aluminium residue: A review, *Waste Manag. Res.* 30 (2012) 474-484.
- 6 M.S.R. Sarker, M.Z. Alam, M.R. Qadir, M.A. Gafur, M. Moniruzzaman, Extraction and characterization of alumina nanopowders from aluminum dross by acid dissolution process, *Int. J. Miner. Metall. Mater.* 22 (2015) 429-436.
- 7 A. Gil, S.A. Korili, Management and valorization of aluminum saline slags: Current status and future trends, *Chem. Eng. J.* 289 (2016) 74-84.
- 8 A. Gil, E. Arrieta, M.A. Vicente, S.A. Korili, Synthesis and CO₂ adsorption properties of hydrotalcite-like compounds prepared from aluminum saline slag wastes, *Chem. Eng. J.* 334 (2018) 1341-1350.
- 9 M. Yoldi, E.G. Fuentes-Ordoñez, S.A. Korili, A. Gil, Zeolite synthesis from aluminum saline slag waste, *Powder Technol.* 366 (2020) 175-184.
- 10 L. Santamaría, M. López-Aizpún, M. García-Padial, M.A. Vicente, S.A. Korili, A. Gil, Zn-Ti-Al layered double hydroxides synthesized from aluminum saline slag wastes as efficient drug adsorbents, *Appl. Clay Sci.* 187 (2020) 105486.
- 11 M. Tian, X.D. Wang, T. Zhang, Hexaaluminates: a review of the structure, synthesis and catalytic performance, *Catal. Sci. Technol.* 6, (2016) 1984-2004.
- 12 Y. Zhang, X. Wang, Y. Zhu, X. Liu, T. Zhang, Thermal evolution crystal structure and Fe crystallographic sites in LaFe_xAl_{12-x}O₁₉ hexaaluminates, *J. Phys. Chem. C* 118 (2014) 10792-10804.
- 13 M. Tian, A. Wang, X. Wang, Y. Zhu, T. Zhang, Effect of large cations (La³⁺ and Ba²⁺) on the catalytic performance of Mn-substituted hexaaluminates for N₂O decomposition, *Appl. Catal. B Environ.* 92 (2009) 437-444.
- 14 R. Kikuchi, Y. Tanaka, K. Sasaki, K. Eguchi, High temperature catalytic combustion of methane and propane over hexaaluminate catalysts: NO_x emission characteristics, *Catal. Today* 83 (2003) 223-231.
- 15 S. Nugroho, Z.-C. Chen, A. Kawasaki, M.O.D. Jarligo, Solid-state synthesis and

- formation mechanism of barium hexaaluminate from mechanically activated $\text{Al}_2\text{O}_3\text{-BaCO}_3$ powder mixtures, *J. Alloys Comp.* 502 (2010) 466-471.
- 16 S.I. Woo, S.K. Kang, J.M. Sohn, Effect of water content in the precursor solution on the catalytic property and stability of $\text{Sr}_{0.8}\text{La}_{0.2}\text{MnAl}_{11}\text{O}_{19}$ high-temperature combustion catalyst, *Appl. Catal. B Environ* 18 (1998) 317-324.
 - 17 J.M. Sohn, S.K. Kang, S.I. Woo, Catalytic properties and characterization of Pd supported on hexaaluminate in high temperature combustion, *J. Mol. Catal. A Chemical* 186 (2002) 135-144.
 - 18 L. Majocchi, G. Groppi, C. Cristiani, P. Forzatti, L. Basini, A. Guarinoni, Partial oxidation of methane to synthesis gas over Rh-hexaaluminate-based catalysts, *Catal. Letters* 65 (2000) 49-56.
 - 19 J. Zheng, X. Ren, Y. Song, X. Ge, Effect of preparation methods and mirror plane cation on the catalytic property of $\text{AMnAl}_{11}\text{O}_{19-x}$ (A =K, Ca) catalysts, *Catal. Comm.* 10 (2009) 1226-1229.
 - 20 P.K. Sahu, B.D. Kulkarni, R.B. Khomane, S.A. Pardhy, U.D. Phalgune, P. Rajmohanam, R. Pasricha, Barium hexaaluminate nanowhiskers synthesized by novel sol-gel process in reverse micellar media, *Chem. Comm.* (2009) 1876-1877.
 - 21 J. Schicks, D. Neumann, U. Specht, C. Vesper, Nanoengineered catalysts for high-temperature methane partial oxidation, *Catal. Today* 81 (2003) 287-296.
 - 23 W. Chu, W. Yang, L. Lin, The partial oxidation of methane to syngas over the nickel-modified hexaaluminate catalysts $\text{BaNi}_y\text{Al}_{12-y}\text{O}_{19-\delta}$, *Appl. Catal. A General* 235 (2002) 39-45.
 - 22 Z. Xu, M. Zhen, Y. Bi, K. Zhen, Catalytic properties of Ni modified hexaaluminates $\text{LaNi}_y\text{Al}_{12-y}\text{O}_{19-\delta}$ for CO_2 reforming of methane to synthesis gas, *Appl. Catal. A General* 198 (2000) 267-273.
 - 24 K. Zhang, G. Z'hou, J. Li, K. Zhen, T. Cheng, Effective additives of A (Ce, Pr) in modified hexaaluminate $\text{La}_x\text{A}_{1-x}\text{NiAl}_{11}\text{O}_{19}$ for carbon dioxide reforming of methane, *Catal. Letters* 130 (2009) 246-253.
 - 25 J. Xu, Z. Tian, J. Wang, Y. Xu, Z. Xu, L. Lin, Hydrothermal synthesis of La-Mn-Hexaaluminates for the catalytic combustion of methane, *Korean J. Chem. Eng.* 20 (2003) 217-221.
 - 26 J. Gao, C. Jia, M. Zhang, F. Gu, G. Xu, Z. Zhong, F. Su, Template preparation of high-surface-area barium hexaaluminate as nickel catalyst support for improved CO methanation, *RSC Advance* 3 (2013) 18156-18163.
 - 27 M. Santiago, J.C. Groen, J. Pérez-Ramírez, Carbon-templated hexaaluminates with enhanced surface area and catalytic performance, *J. Catal.* 257 (2008) 152-162.
 - 28 T. Roussi re, K.M. Schelkle, S. Titlbach, G. Wasserschaff, A. Milanov, G. Cox, E. Schwab, O. Deutschmann, L. Schulz, A. Jentys, J. Lercher, S.A. Schunk, Structure-

- activity relationships of nickel-hexaaluminates in reforming reactions Part I: controlling nickel nanoparticle growth and phase formation, *ChemCatChem*. 6 (2014) 1438-1446.
- 29 T. Roussière, L. Schulz, K.M. Schelkle, G. Wasserschaff, A. Milanov, E. Schwab, O. Deutschmann, A. Jentys, J. Lercher, S.A. Schunk, Structure–activity relationships of nickel–hexaaluminates in reforming reactions part II: activity and stability of nanostructured nickel–hexaaluminate-based catalysts in the dry reforming of methane, *ChemCatChem*. 6 (2014) 1447-1452.
- 30 M. Bellotto, G. Artioli, C. Cristiani, P. Forzatti, G. Groppi, On the crystal structure and cation valence of Mn in Mn-substituted Ba- β -Al₂O₃, *J. Catal.* 179 (1998) 597–605.
- 31 G. Groppi, C. Cristiani, P. Forzatti, Preparation, characterisation and catalytic activity of pure and substituted La-hexaaluminate systems for high temperature catalytic combustion, *Appl. Catal. B Environ.* 35 (2002) 137-148.
- 32 M. Santiago, M.A.G. Hevia, J. Pérez-Ramírez, Evaluation of catalysts for N₂O abatement in fluidized-bed combustion, *Appl. Catal. B Environ.* 90 (2009) 83-88.
- 33 P. Artizzu-Duart, J.M. Millet, N. Guilhaume, L. Garbowski, M. Primet, Catalytic combustion of methane on substituted lanthanum hexaaluminates, *Catal. Today* 59 (2000) 163-177.
- 34 Y. Liu, Z. Xu, T. Cheng, G. Zhou, J. Wang, W. Li, Y. Bi, K. Zhen, Studies on carbon deposition on hexaaluminate LaNiAl₁₁O₁₉ catalysts during CO₂ reforming of methane, *Kinet. Catal.* 43 (2002) 522-527.
- 35 R. Gadow, M. Lischka, Lanthanum hexaaluminate - novel thermal barrier coatings for gas turbine applications - materials and process development, *Surf. Coatings Technol.* 151-152 (2002) 392-399.
- 36 J. Wigren, L. Pejryd, Thermal barrier coatings - Why, how, where and where to, in: *Proc. Int. Therm. Spray Conf.* (1998) 1531-1542.
- 37 C.J. Friedrich, R. Gadow, T. Schirmer, Lanthane aluminate - A new material for atmospheric plasma spraying of advanced thermal barrier coatings, *J. Therm. Spray Technol.* 10 (2001) 592-598.
- 38 R.R. Rao, L. Mariappan, Combustion synthesis and characterisation of lanthanum hexa-aluminate, *Adv. Appl. Ceram.* 104 (2013) 268-271.
- 39 J.-G. Park, A.N. Cormack, Defect structures and nonstoichiometry in lanthanum hexa-aluminate, *J. Eur. Ceram. Soc.* 19 (1999) 2249-2256.
- 40 B.A. Vázquez, A. Caballero, P. Pena, Quaternary system Al₂O₃-CaO-MgO-SiO₂: I, study of the crystallization volume of Al₂O₃, *J. Am. Ceram. Soc.* 86 (2003) 2195-2199.
- 41 B.A. Vázquez, A. Caballero, P. Pena, Quaternary system Al₂O₃-CaO-MgO-SiO₂: II Study of the crystallization volume of MgAl₂O₄, *J. Am. Ceram. Soc.* 88 (2005) 1949-1957.

- 42 A.C. Bento, E.T. Kubaski, T. Sequinel, S.A. Pianaro, J.A. Varela, S.M. Tebcherani, Glass foam of macroporosity using glass waste and sodium hydroxide as the foaming agent, *Ceram. Int.* 39 (2013) 2423-2430.
- 43 G. Groppi, C. Cristiani, P. Forzatti, $\text{BaFe}_x\text{Al}_{(12-x)}\text{O}_{19}$ system for high-temperature catalytic combustion: Physico-chemical characterization and catalytic activity, *J. Catal.* 168 (1997) 95-103.
- 44 M.F. Campos, F. Silva, 2015 Application of micromagnetic models for barium ferrite magnets, *Mater. Sci. Forum* 820 (2015) 199-204.
- 45 S. Kane, M. Satalkar, A. Ghosh, D. Phase, R.J. Chaudhary, A. Pasko, M. Lobue, F. Mazaleyrat, Growth and characterization of ferrite film prepared by pulsed laser deposition, *J. Phys.: Conf. Ser.* 365 (2012) 012023.
- 46 S.B. Bankar, N.S. Meshram, N.N. Sarkar, H.S. Ahamad, S.J. Dhobale, K.G. Rewatkar, Synthesis of nanocrystalline $\text{Ca}_2\text{Cu}_2\text{Fe}_{12}\text{O}_{22}$ Y type hexaferrites by the sol-gel combustion method in metal nitrates system, *Ferroelectrics* 526 (2018) 187–192.
- 47 J. Temuujin, M. Aoyama, M. Senna, T. Masuko, C. Ando, H. Kishi, Synthesis of Y-type hexaferrites via a soft mechanochemical route, *J. Solid State Chem.* 177 (2004) 3903-3908.
- 48 Y. Zhu, X. Wang, G. Wu, Y. Huang, Y. Zhang, J. Wang, T. Zhang, Evolution of Fe crystallographic sites from barium hexaaluminate to hexaferrite, *J. Phys. Chem. C* 116 (2012) 671-680.
- 49 M. Machida, K. Eguchi, H. Arai, Catalytic properties of $\text{BaMAl}_{11}\text{O}_{19-\alpha}$ (M = Cr, Mn, Fe, Co, and Ni) for high-temperature catalytic combustion, *J. Catal.* 120 (1989) 377-386.
- 50 G. Groppi, M. Bellosto, C. Cristiani, P. Forzatti, P.L. Villa, Preparation and characterization of hexaaluminate-based materials for catalytic combustion, *Appl. Catal. A General* 104 (1993) 101-108.
- 51 J. Wang, Z. Fan, J. Xu, Y. Xu, Z. Xu, L. Lin, Preparation of Mn substituted La-hexaaluminate catalysts by using supercritical drying, *Catal. Today* 83 (2003) 213-222.
- 52 X. An, H. Xiang, Y. Li, H. Wan, Z. Tao, T. Li, Y. Yang, Effect of manganese on a potassium-promoted iron-based Fischer-Tropsch synthesis catalyst, *Catal. Letters* 114 (2007) 161-168.
- 53 I.R. Leith, M.G. Howden, Temperature-programmed reduction of mixed iron-manganese oxide catalysts in hydrogen and carbon monoxide, *Appl. Catal.* 37 (1988) 75-92.
- 54 A.J. Zarur, H.H. Hwu, J.Y. Ying, Reverse microemulsion-mediated synthesis and structural evolution of barium hexaaluminate nanoparticles, *Langmuir* 16 (2000) 3042-3049.
- 55 P. Jana, P. Jayan, S. Mandal, K. Biswas, Microstructural design of neodymium-

- doped lanthanum-magnesium hexaaluminate synthesized by aqueous sol-gel process, *J. Mater. Sci.* 50 (2015) 344-353.
- 56 M.T. Tsai, Hydrolysis and condensation of forsterite precursor alkoxides: Modification of the molecular gel structure by acetic acid, *J. Non. Cryst. Solids* 298 (2002) 116-130.
- 57 H.R. Rezaie, R. Naghizadeh, F. Arianpour, R. Ghasemzadeh, S. Eslami, An evaluation on sol-gel chemical processing of refractory barium hexa aluminate fibrous structures, *J. Ceram. Process. Res.* 10 (2009) 148-151.
- 58 J. Li, E.A. Medina, J.K. Stalick, A.W. Sleight, M.A. Subramanian, Colored oxides with hibonite structure: A potential route to non-cobalt blue pigments, *Prog. Solid State Chem.* 44 (2016) 107-122.
- 59 Y. Kawashima, T. Handa, H. Takeuchi, M. Okumura, Effects of polyethylene glycol on the size of agglomerated crystals of phenytoin prepared by the spherical crystallization technique, *Chem. Pharm. Bull.* 34 (1986) 3403-3407.

Captions

Table 1. Chemical composition of the solution after acid extraction.

Table 2. Chemical composition of the aluminum saline slags before aluminum extraction.

Table 3. Chemical composition of the La-hexaaluminate synthesized.

Table 4. BET specific surface areas, pore volumes and crystallite sizes of the sample synthesized at several temperatures. The structure of the phase that predominates at each temperature is also included.

Figure 1. (A) XRD pattern of the hexaaluminate synthesized using La and Al extracted from saline slags, AD method (the hibonite pattern is included for comparison). (B) XRD patterns of the hexaaluminate calcined at several temperatures and evolution of the phases. (a) 873 K, (b) 1073 K, (c) 1273 K, and (d) 1473 K. Symbols: ▼ Spinel pattern 00-021-1152, ▼ Hibonite pattern 00-007-0785.

Figure 2. XRD patterns of samples synthesized with commercial precursors (AD method) and calcined at 1473 K for 2 h (various patterns are included for comparison). AD1, molar La/Al ratio of 1:11, AD2, molar La/Al/Ni ratio of 1:15:0.25.

Figure 3. SEM micrographs and EDX-mapping analysis of the hexaaluminate synthesized at 1473 K. The mass surface and the atomic concentrations are also included.

Figure 4. Evolution of S_{BET} with calcination temperature.

Figure 5. (A) Evolution of S_{BET} with crystallite size. (B) Krigin Gridding interpolation.

Figure 6. TPR patterns of the hexaaluminate calcined at several temperatures.

Figure 7. FTIR spectra of the hexaaluminate calcined at several temperatures.

Figure 8. TEM-SAED images of the hexaaluminate synthesized at 1473 K. The superficial patterns and the interplanar distances in the structure can be observed.

Table 1. Chemical composition of the solution after acid extraction.

Composition	Al	Fe	Ca	Mg
g/cm^3	8.96 ± 0.13	0.85 ± 0.01	0.76 ± 0.01	0.49 ± 0.01

Journal Pre-proof

Table 2. Chemical composition of the aluminum saline slags before aluminum extraction.

Composition	Na ₂ O	MgO	Al ₂ O ₃	SiO ₂	P ₂ O ₅	SO ₃	Cl	K ₂ O	CaO
<i>wt.%</i>	0.77	6.49	55.23	4.23	0.07	0.41	0.47	0.50	2.12

Composition	TiO ₂	Cr	MnO	Fe ₂ O ₃	Ba	Cu	F	Zn	
<i>wt.%</i>	0.65	0.07	0.26	1.25	0.07	0.51	0.41	0.17	

Table 3. Chemical composition of the La-hexaaluminate synthesized.

	A			B _x					Al _{12-x}	O _{19-δ}
Oxides	La ₂ O ₃	CaO	Na ₂ O	MgO	Fe ₂ O ₃	Si ₂ O	Ti ₂ O	MnO	Al ₂ O ₃	O
wt. %	20.49	3.52	2.40	3.90	1.67	9.25	0.34	0.28	56.91	
mol. %	7.57	3.78	4.66	5.82	1.26	9.27	0.26	0.19	67.19	
Atom	La	Ca	Na	Mg	Fe	Si	Ti	Mn	Al	O
LHA composition	1.08	0.54	0.67	0.83	0.18	1.32	0.03	0.02	9.06	19-δ

Table 4. BET specific surface areas, pore volumes and crystallite sizes of the sample synthesized at several temperatures. The structure of the phase that predominates at each temperature is also included.

Temperature (K)	S_{BET} (m^2/g)	V_p (cm^3/g)	Crystallite size (nm)	Phase structure
873	59	0.216	3.52	Spinel
1073	28	0.154	3.97	Spinel >> LHA
1273	17	0.056	5.30	LHA >> Spinel
1373	9	0.056	8.70	LHA >> Spinel
1473	1	0.003	9.80	LHA

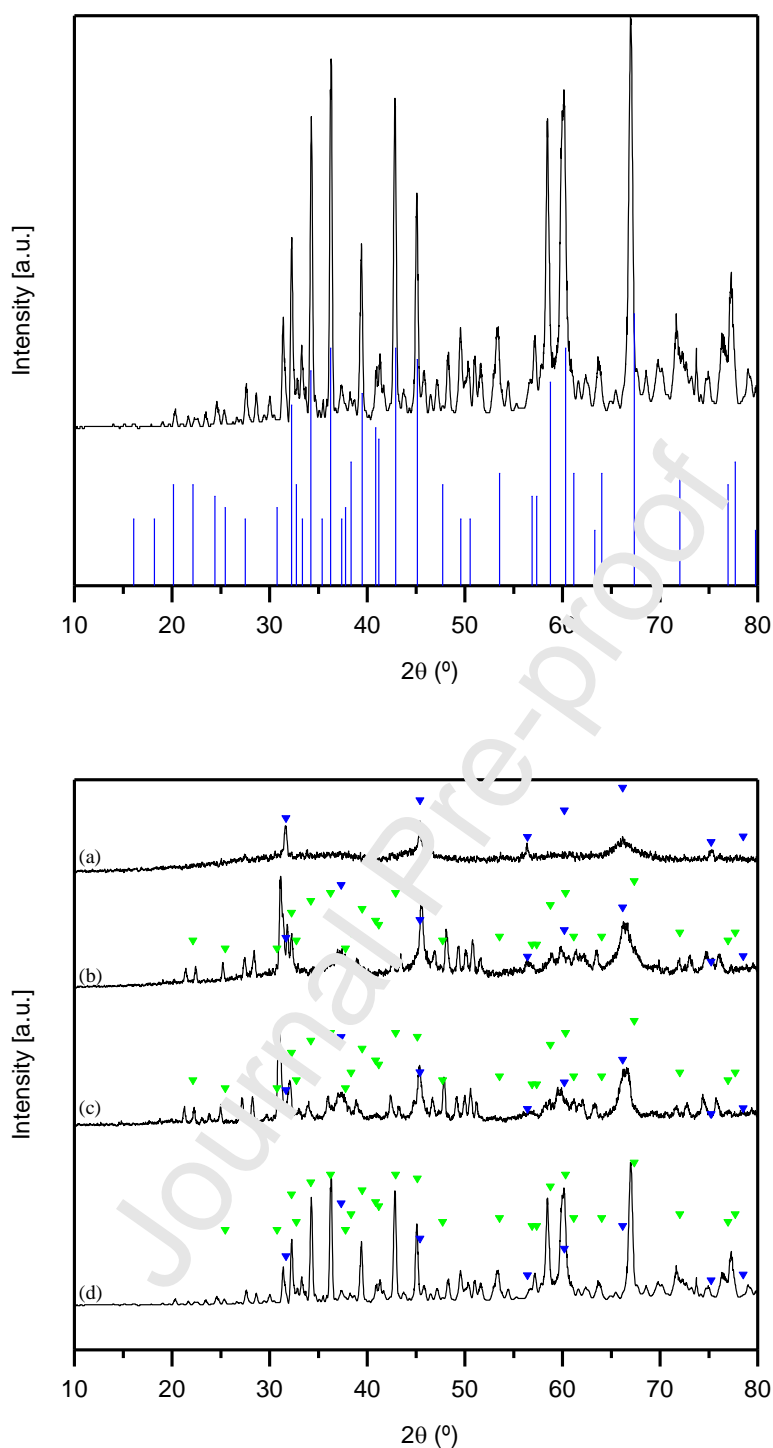


Figure 2. (A) XRD pattern of the hexaaluminate synthesized using La and Al extracted from saline slags, AD method (the hibonite pattern is included for comparison). (B) XRD patterns of the hexaaluminate calcined at several temperatures and evolution of the phases. (a) 873 K, (b) 1073 K, (c) 1273 K, and (d) 1473 K. Symbols: ▼ Spinel pattern 00-021-1152, ▼ Hibonite pattern 00-007-0785

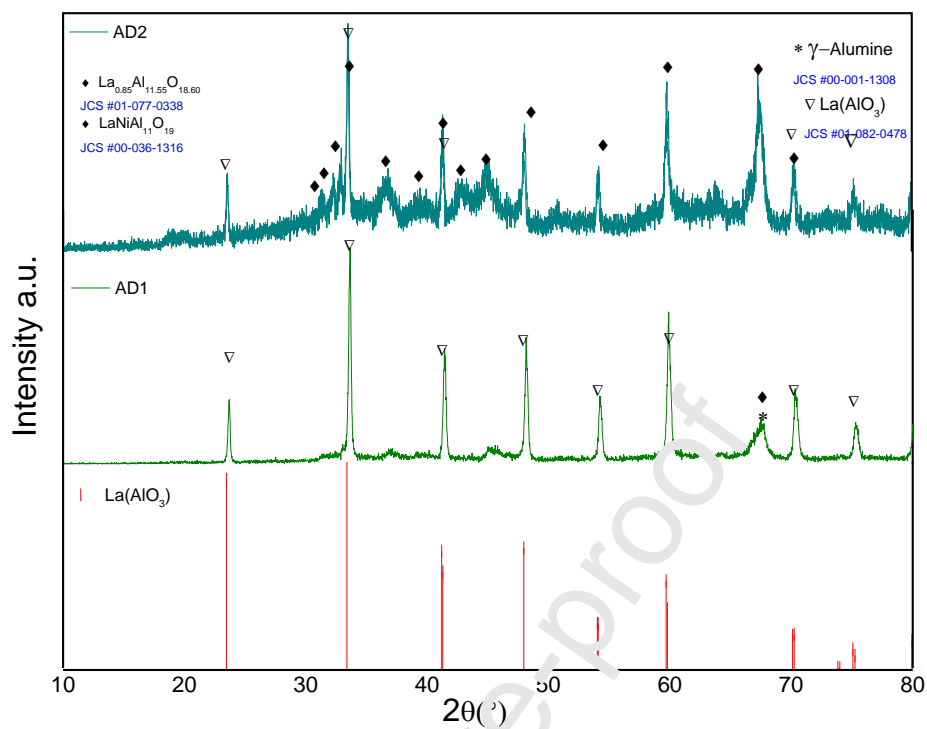
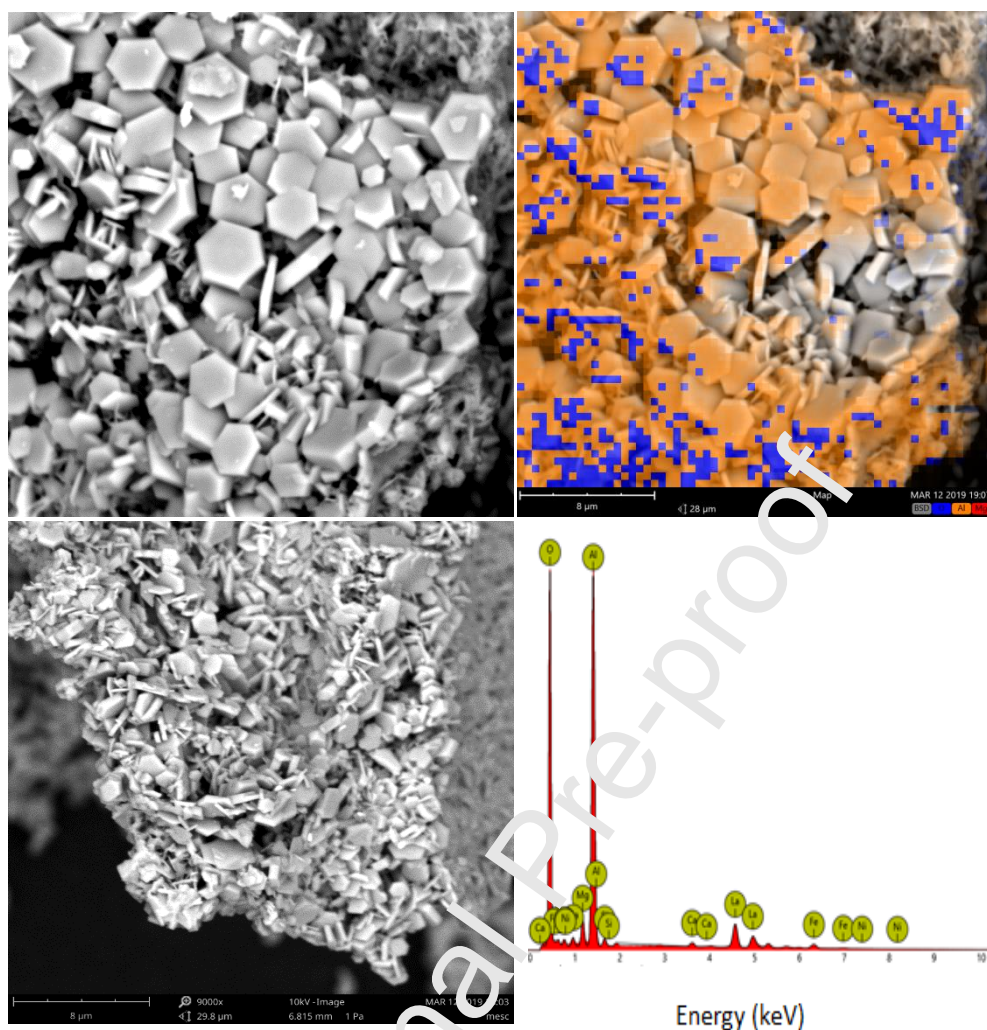


Figure 2. XRD patterns of sample synthesized with commercial precursors (AD method) and calcined at 1473 K for 2 h (various patterns are included for comparison). AD1, molar La/Al ratio of 1:11, AD2, molar La/Al/Ni ratio of 1:15:0.25.



	O	Al	La	Mg	Fe	Na	Si	Ca
% mass concentration	36.28 ±0.18	30.06 ±0.15	25.56 ±0.12	2.44 ±0.01	2.35 ±0.01	0.93 ±0.005	0.78 ±0.004	0.59 ±0.003
% atomic concentration	59.35 ±0.30	29.95 ±0.15	4.8 ±0.02	2.62 ±0.01	1.1 ±0.006	1.06 ±0.005	0.73 ±0.004	0.38 ±0.002

Figure 3. SEM micrographs and EDX-mapping analysis of the hexaaluminate synthesized at 1473 K. The mass surface and the atomic concentrations are also included.

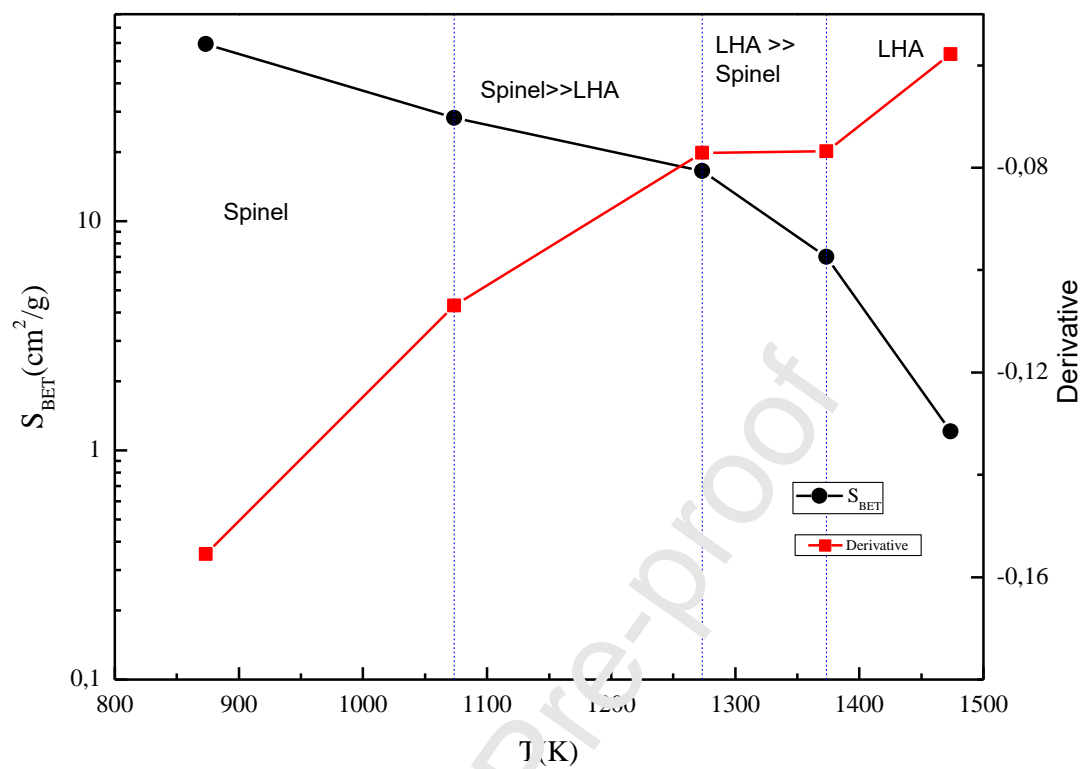


Figure 4. Evolution of S_{BET} with calcination temperature.

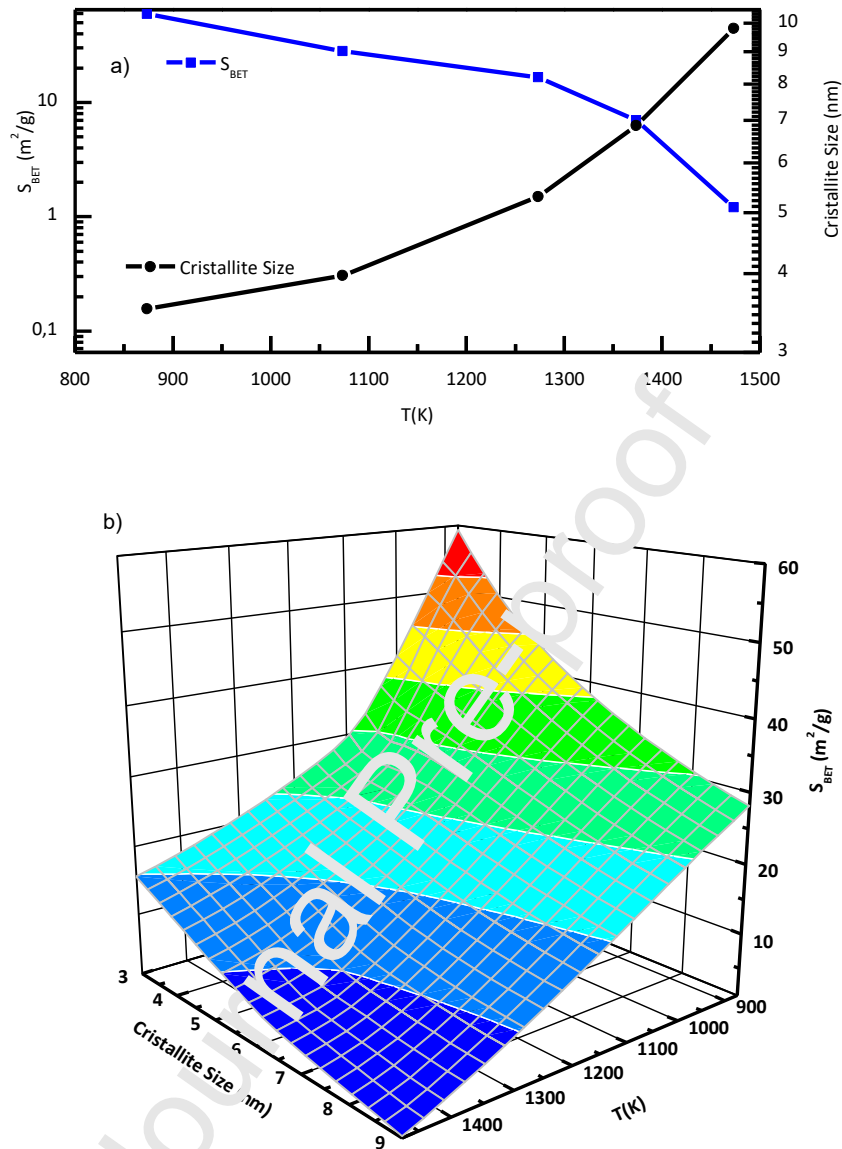


Figure 5. (A) Evolution of S_{BET} with crystallite size. (B) Krigin Gridding interpolation.

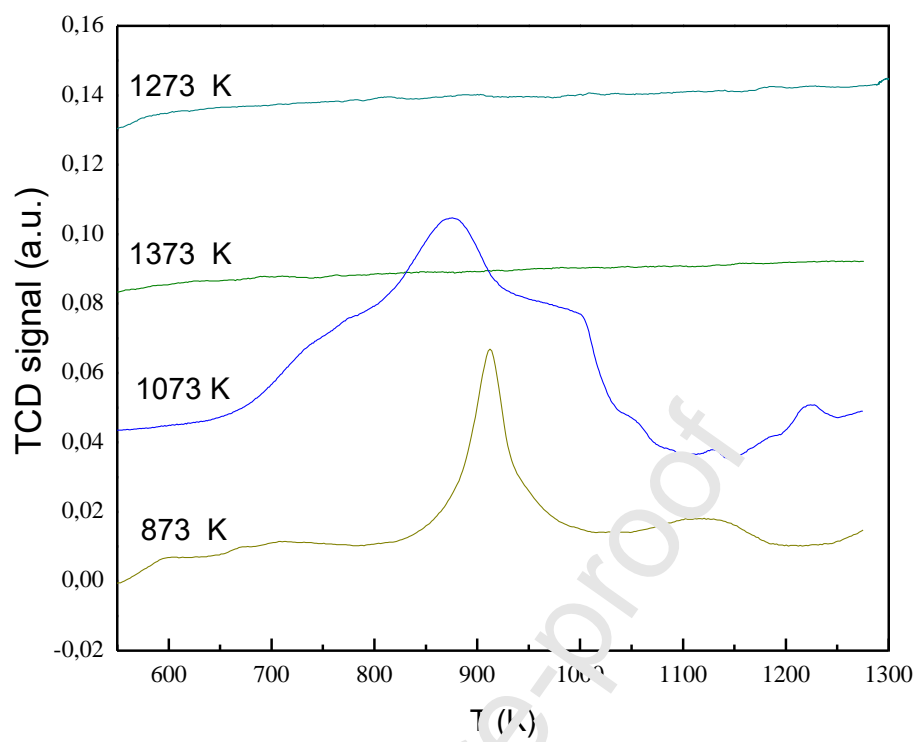


Figure 6. TPR patterns of the hexaaluminate calcined at several temperatures.

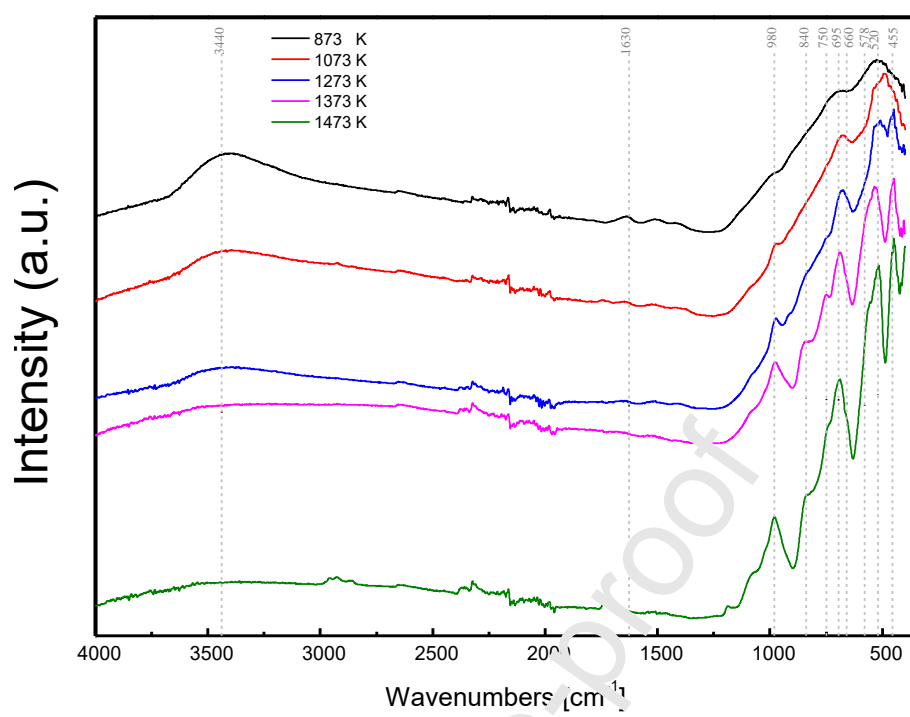


Figure 7. FTIR spectra of the hexaalumina calcined at several temperatures.

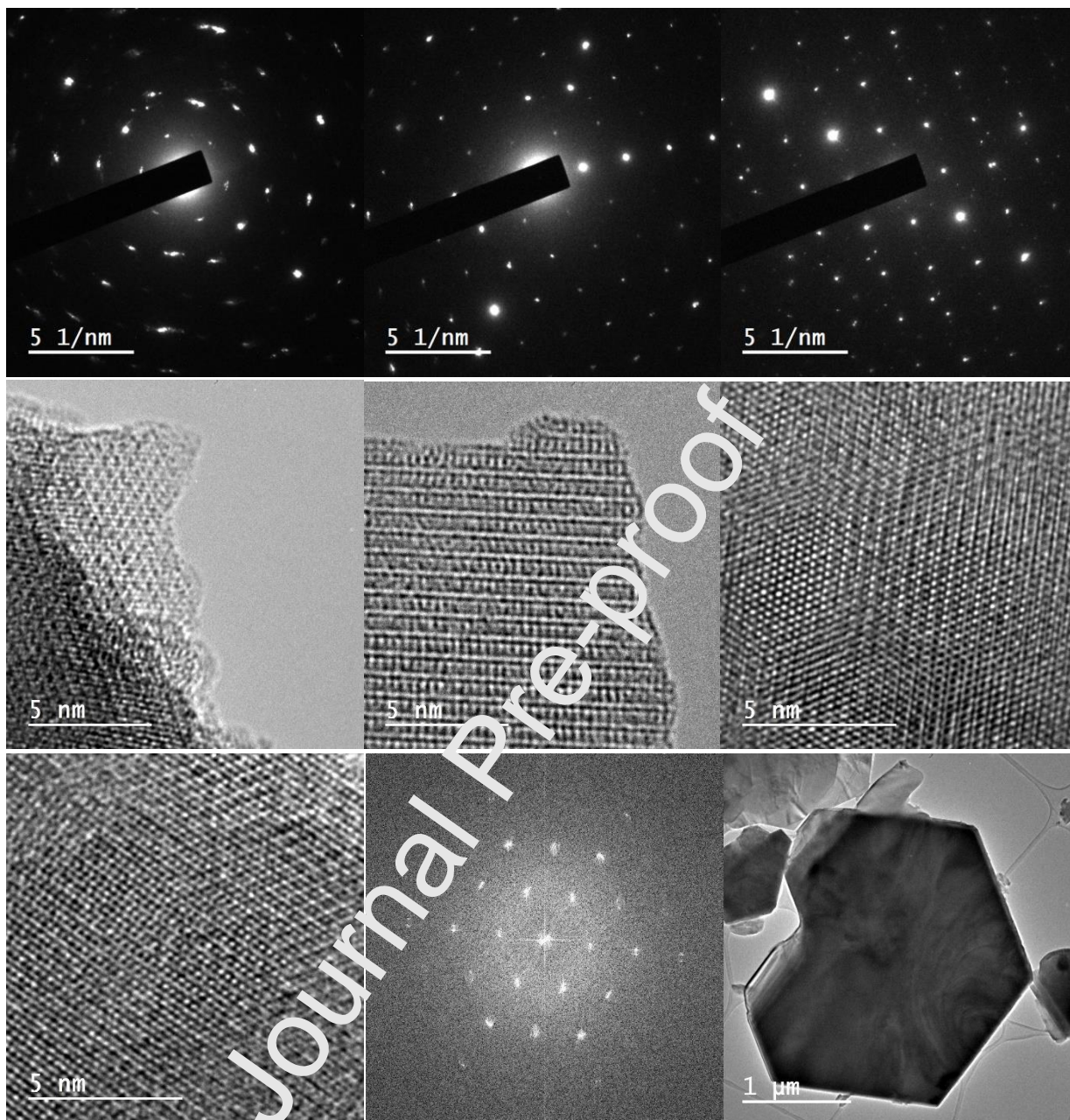


Figure 8. TEM-SAED images of the hexaaluminate synthesized at 1473 K. The superficial patterns and the interplanar distances in the structure can be observed.

Credit authorship contribution statement

In this work, Mr J.J. Torrez-Herrera carried out the experiments, analyzed results and involved in writing/revising manuscript; Dr E.G. Fuentes-Ordoñez and Prof S.A. Korili analyzed results and involved in writing/revising manuscript; Prof. A. Gil provided conceptualization, project administration, manuscript writing and revision guidance.

Journal Pre-proof

Author declaration

[Instructions: Please check all applicable boxes and provide additional information as requested.]

1. Conflict of Interest

Potential conflict of interest exists:

We wish to draw the attention of the Editor to the following facts, which may be considered as potential conflicts of interest, and to significant financial contributions to this work:

The nature of potential conflict of interest is described below:

No conflict of interest exists.

We wish to confirm that there are no known conflicts of interest associated with this publication and there has been no significant financial support for this work that could have influenced its outcome.

2. Funding

Funding was received for this work.

All of the sources of funding for the work described in this publication are acknowledged below:

[List funding sources and their role in study design, data analysis, and result interpretation]

No funding was received for this work.

3. Intellectual Property

We confirm that we have given due consideration to the protection of intellectual property associated with this work and that there are no impediments to publication, including the timing of publication, with respect to intellectual property. In so doing we confirm that we have followed the regulations of our institutions concerning intellectual property.

4. Research Ethics

We further confirm that any aspect of the work covered in this manuscript that has involved human patients has been conducted with the ethical approval of all relevant bodies and that such approvals are acknowledged within the manuscript.

IRB approval was obtained (required for studies and series of 3 or more cases)

Written consent to publish potentially identifying information, such as details or the case and photographs, was obtained from the patient(s) or their legal guardian(s).

5. Authorship

The International Committee of Medical Journal Editors (ICMJE) recommends that authorship be based on the following four criteria:

1. Substantial contributions to the conception or design of the work; or the acquisition, analysis, or interpretation of data for the work; AND
2. Drafting the work or revising it critically for important intellectual content; AND
3. Final approval of the version to be published; AND
4. Agreement to be accountable for all aspects of the work in ensuring that questions related to the accuracy or integrity of any part of the work are appropriately investigated and resolved.

All those designated as authors should meet all four criteria for authorship, and all who meet the four criteria should be identified as authors. For more information on authorship, please see <http://www.icmje.org/recommendations/browse/roles-and-responsibilities/defining-the-role-of-authors-and-contributors.html#two>.

All listed authors meet the ICMJE criteria. ^[SEP] We attest that all authors contributed significantly to the creation of this manuscript, each having fulfilled criteria as established by the ICMJE.

One or more listed authors do(es) not meet the ICMJE criteria.

We believe these individuals should be listed as authors because:

[Please elaborate below] ^[SEP]

We confirm that the manuscript has been read and approved by all named authors.

We confirm that the order of authors listed in the manuscript has been approved by all named authors.

6. Contact with the Editorial Office

The Corresponding Author declared on the title page of the manuscript is:

Antonio Gil

This author submitted this manuscript using his/her account in EVISE.

We understand that this Corresponding Author is the sole contact for the Editorial process (including EVISE and direct communications with the office). He/she is responsible for communicating with the other authors about progress, submissions of revisions and final approval of proofs.

We confirm that the email address shown below is accessible by the Corresponding Author, is the address to which Corresponding Author's EVISE account is linked, and has been configured to accept email from the editorial office of American Journal of Ophthalmology Case Reports:


andoni@unavarra.es

Someone other than the Corresponding Author declared above submitted this manuscript from his/her account in EVISE:

[Insert name below]

We understand that this author is the sole contact for the Editorial process (including EVISE and direct communications with the office). He/she is responsible for communicating with the other authors, including the Corresponding Author, about progress, submissions of revisions and final approval of proofs.

We the undersigned agree with all of the above.

Author's name (Fist, Last)	Signature	Date
1. Antonio Gil		January 13 th , 2019
2. _____	_____	_____
3. _____	_____	_____
4. _____	_____	_____
5. _____	_____	_____
6. _____	_____	_____
7. _____	_____	_____
8. _____	_____	_____
9. _____	_____	_____
10. _____	_____	_____

Journal Pre-proof

- ▶ Pure phases of La-hexaaluminates at low temperature from saline slags were obtained.
- ▶ Acid aluminum extracted from saline slags was used in the synthesis of La-hexaaluminates.
- ▶ The synthesis of hexaaluminate from an industrial waste was presented for the first time.

Journal Pre-proof